In Situ Sputtering From the Micromanipulator to Enable Cryogenic Preparation of Specimens for Atom Probe Tomography by Focused-Ion Beam

James O Douglas, Michele Conroy, Finn Giuliani, Baptiste Gault

DECTRIS
detecting the future
High dynamic range and single electron sensitivity combined with extreme speed (120,000 fps) for your 4D STEM experiment.


Downloaded from https://academic.oup.com/mam/article/29/3/1009/7103332 by guest on 12 September 2023

Microscopy and Microanalysis, 2023, **29**, 1009–1017
https://doi.org/10.1093/micmic/ozad020
Advance access publication 4 April 2023
Original Article

Microscopy AND Microanalysis

In Situ Sputtering From the Micromanipulator to Enable Cryogenic Preparation of Specimens for Atom Probe Tomography by Focused-Ion Beam

James O. Douglas[1], Michele Conroy[1], Finn Giuliani[1], and Baptiste Gault[1,2,*]

[1]*Department of Materials, Royal School of Mines, Imperial College London, Prince Consort Road, London SW7 2BP, UK*
[2]*Max-Planck-Institut für Eisenforschung GmbH, Max-Planck-Str. 1, 40237 Düsseldorf, Germany*

***Corresponding author:** Baptiste Gault, E-mail: b.gault@mpie.de*

Abstract

Workflows have been developed in the past decade to enable atom probe tomography analysis at cryogenic temperatures. The inability to control the local deposition of the metallic precursor from the gas-injection system (GIS) at cryogenic temperatures makes the preparation of site-specific specimens by using lift-out extremely challenging in the focused-ion beam. Schreiber et al. exploited redeposition to weld the lifted-out sample to a support. Here, we build on their approach to attach the region-of-interest and additionally strengthen the interface with locally sputtered metal from the micromanipulator. Following standard focused-ion beam annular milling, we demonstrate atom probe analysis of Si in both laser pulsing and voltage mode, with comparable analytical performance as a presharpened microtip coupon. Our welding approach is versatile, as various metals could be used for sputtering, and allows similar flexibility as the GIS in principle.

Key words: atom probe tomography, cryogenic preparation, focused-ion beam, *in situ* sputtering

Introduction

Atom probe tomography (APT) is a spatially resolved time-of-flight mass spectrometry analysis technique, where ions are field-evaporated from the apex of a nanoscale needle-shaped specimen through the application of voltage or laser pulses (Gault et al., 2021). APT-analyzed volumes are typically of the order of $50 \times 50 \times 80$ nm and are able to give a combination of high-compositional, in the tens of appm (Haley et al., 2020), and high-spatial resolution in the range below a nanometer in three dimensions (de Geuser & Gault, 2020; Jenkins et al., 2020), allowing for the characterization of complex nanoscale features in three dimensions.

The range of materials that APT has been applied to has extended from metals and alloys (Blavette et al., 2000; Ringer, 2006; Marquis et al., 2013) to semiconductor devices (Kelly et al., 2007), insulators (Clark et al., 2016), geological materials (Saxey et al., 2018), and biological materials (Grandfield et al., 2022). The broadening of the field of application has been primarily enabled by the spread of specimen preparation by focused-ion beam (FIB) (Larson et al., 1998; Prosa & Larson, 2017). The combination with a scanning electron microscope (SEM-FIB) has permitted the precise positioning of a specific, nanoscale region of interest within the apex of the needle-shaped specimen and this approach is now considered the routine preparation route for APT (Felfer et al., 2012) and also for transmission electron microscopy (TEM) (Mayer et al., 2007).

This process is typically carried out at room temperature as the commonly used lift-out methodology requires the use of a gas injection system (GIS) projecting a precursor gas over the sample (Thompson et al., 2007). The precursor is decomposed by the secondary electrons reemitted by the surface illuminated by an incoming electron or ion beam over specific regions. When using an organometallic, the decomposition products can form a mechanically stable and electrically conducting material (Park et al., 1999; van Dorp et al., 2009). The GIS is used to deposit protective material on defined areas, prior to FIB milling, to reduce ion beam damage during sample preparation, and also to attach, or weld, micromanipulators to APT cantilevers or TEM lamellae for lift-out, and attach them onto an appropriate support structure. The deposited material has a variable metal content and distribution depending on the precursor gas and the parameters of the incident beam. There has been work on increasing the metal content through precursor gas selection (Diercks et al., 2017) but a significant level of carbon is retained within the deposited material.

This approach has been applied to a wide variety of material systems that are stable at room temperature and ambient environmental conditions. In recent years, advances in instrumentation and increased interest in the analysis of materials that require cryogenic conditions have led to new avenues and associated challenges in nanoscale characterization.

Cryogenic sample preparation for TEM has revolutionized the field of biological sciences, with the 2017 Nobel prize in Chemistry being awarded to the development of cryo-electron microscopy for the high-resolution structure determination of biomolecules in solution (Anon, 2017). The cryogenic vitrification of hydrated biological materials has facilitated maintaining the samples pristine state, and thus avoiding the dehydration and reducing radiation-induced damage of the

Received: November 10, 2022. **Revised:** January 13, 2023. **Accepted:** February 5, 2023
© The Author(s) 2023. Published by Oxford University Press on behalf of the Microscopy Society of America.
This is an Open Access article distributed under the terms of the Creative Commons Attribution License (https://creativecommons.org/licenses/by/4.0/), which permits unrestricted reuse, distribution, and reproduction in any medium, provided the original work is properly cited.

Downloaded from https://academic.oup.com/mam/article/29/3/1009/7103332 by guest on 12 September 2023

sample during analysis (Taylor & Glaeser, 1974, 1976). In the pivotal study by Henderson et al. (1990), he emphasized the point that the cryogenic specimen–preparation improvements facilitated the development of cryo-EM to a general technique. To date, the most commonly used cryo-TEM sample preparation technique for biological samples is plunge freezing on TEM grids (Dubochet et al., 1982; Dubochet, 2016). More recently, the research field of geochemistry utilized this type of cryogenic TEM sample preparation to answer fundamental physical material science question such as crystal growth and dissolution mechanisms for hydrated materials (Kumar et al., 2008; Revealed et al., 2010; Conroy et al., 2017; Zhu et al., 2021). The use of cryogenic sample preparation for TEM has become "routine" for many research fields but understanding the transfer of experimental observations to real-world interfaces and material performances are shared challenges in both biological and material sciences. Zachman et al. showed the first site-specific cryogenic FIB sample preparation for TEM of a solid–liquid interfaces of a battery (Zachman et al., 2018).

For APT, it has been shown that cryogenic FIB milling of specimens reduces ion damage and reduces hydrogen ingress during the final stages of specimen sharpening or thinning (Chang et al., 2019), which has been instrumental in allowing the investigation of hydrogen distribution in e.g., Ti (Chang et al., 2019) or Zr alloys (Mouton et al., 2021). At lower temperatures, some of the deleterious effects of the chemically active, most commonly used gallium, for example its diffusion to structural defects in aluminum, can also be avoided (Lilensten & Gault, 2020).

Cryogenic FIB sample preparation was often limited to the final stage of APT sample sharpening or TEM lamellae thinning as performing the full lift-out is challenging. A major challenge with a full cryogenic workflow is that the precursor gas deposits rapidly onto any exposed surface cooled below its condensation temperature (Perea et al., 2017), leading to uncontrolled uniformity and thickness. Although this condensed material can be locally "cured" to a conducting solid material through the application of an electron beam or ion beam, this requires care to ensure the material is "cured" for the full thickness and does not contain any residual condensed gas that may expand upon warming (Parmenter & Nizamudeen, 2020). This larger-scale deposition is extremely quick and has been proposed to reduce time for such areas as electron beam lithography (Salvador-Porroche et al., 2020), but for the purposes of APT sample preparation (Córdoba et al., 2019; Orús et al., 2021), it has limited application due to the lack of site specificity and reduction in thickness control.

Reducing or removing completely the possibility to confine the deposition to a specific area makes it impossible to weld the region-of-interest to micromanipulator or support and hence to perform site-specific specimen preparation. The spread of Xe-plasma FIBs (PFIB), which can achieve very high ionic currents and hence allow for the removal of large volumes of materials within reasonable times, has offered opportunities to avoid the lift-out and adapt the "moat approach" (Miller et al., 2005). Halpin et al. introduced this approach (Halpin et al., 2019), later adapted for target grain boundary analysis (Famelton et al., 2021) and for cryogenic temperatures for the analysis of frozen liquids and liquid–solid interfaces (El-Zoka et al., 2020).

The first breakthrough in the preparation of site-specific APT specimens by cryo-lift-out FIB was by Schreiber and co-workers (Schreiber et al., 2018) who used the redeposition from thin FIB cuts across the lifted-out bar and the micromanipulator or sample support (e.g., Si coupon) to weld the parts together. Similar approaches have been used for cryo-specimen preparation for TEM by FIB in the biological sciences (Parmenter & Nizamudeen, 2020). Redeposition of secondary ions sputtered from the material by the incoming primary ion beam can form new layers of material by mixing together with ions from the primary beam (Matteson et al., 2002; Rajsiri et al., 2002; Cairney & Munroe, 2003). Redeposition has already been used to create welds for lift-outs (Montoya et al., 2007; Kuba et al., 2020) or fill pores to facilitate further specimen preparation (Zhong et al., 2020). These approaches make use of cryogenically cooled micromanipulators as well as the cryo-stage, which are not as readily available apart from on dedicated systems. It is also expected that the mechanical strength, uniformity, and electrical and thermal conductivities of the weld between the support and the material's region of interest will be highly dependent on the redeposition conditions, i.e., a combination of the primary incoming beam's ions, energy, current, and the pattern used, but also the properties of the material being investigated (Winter & Mulders, 2007; Bhavsar et al., 2012).

Here, aiming to facilitate the future establishment of standardized and reproducible fully cryogenic–preparation process flows for APT specimen preparation, we introduce a cryogenic lift-out process. This has the key requirement of a controlled, localized deposition of a mechanically stable and conductive material. We demonstrate a process flow for a fully cryogenic, GIS-free lift-out, mounting, and sharpening of viable atom probe samples with sufficient mechanical stability and electrical conductivity to be analyzed by both laser and voltage pulsing.

Materials and Instruments

A Helios Hydra CX (5CX) plasma FIB from Thermo Fisher Scientific (TFS) with an Aquilos cryo-stage, modified by TFS to accommodate both the conventional dove-tailed holder and the commercial atom probe sample holder from CAMECA, known as pucks. This modification of the stage does hinder the ability of the stage to perform a full 360° rotation, which is critical to the success of the process presented herein. The microscope is also equipped with an easy lift tungsten cryo-micromanipulator. The stage and micromanipulator can be cooled to approximately 90 K by using a circulation of gaseous nitrogen passing through a heat exchanged system within a liquid nitrogen (LN_2) Dewar. A N_2 gas flow of 180 mg/s was used to achieve the base temperature for sample preparation in this work. The FIB column is set at 52° to the electron column. Xe plasma was used throughout this process. A Ferrovac docking station enables transfer into an ultra-high vacuum suitcase that can be cooled via a LN_2 Dewar (Stephenson et al., 2018).

A commercially available high Sb-doped single-crystal silicon micropost array (CAMECA Instruments Inc., Madison, WI, USA) was used as both the substrate and for mounting APT samples for this demonstration, as these arrays are used as reference materials for calibration of the analyses on CAMECA's commercial instruments, for both voltage and laser pulsing due to their mechanical stability and high levels of conductivity. The array was loaded into a Cu clip mount (CAMECA) and placed into a specimen holder, i.e., puck,

Downloaded from https://academic.oup.com/mam/article/29/3/1009/7103332 by guest on 12 September 2023

which was then inserted into the Aquilos stage. Atom probe analysis was performed on a CAMECA Local Electrode Atom Probe 5000 XR equipped with a reflectron and that can host the Ferrovac onto the load lock chamber. Both laser pulsing (30 pJ, 140–200 kHz, 1 ion per 100 pulses on average, 50 K base temperature) and high-voltage (HV) pulsing—sometimes referred to simply as voltage pulsing (20% pulse fraction, 200 kHz, 1 ion per 100 pulses on average, 50 K base temperature)—have been performed.

Methods

For the purpose of demonstrating the feasibility of a full cryogenic lift-out, with a reinforced weld, we prepared for analysis Sb-doped Si specimens using the approach we introduce below, and compared these to the analyses of presharpened microtips. This approach does not require a full cryogenically cooled, vacuum transfer from the Aquilos stage into the LEAP, and specimens were transferred under ambient conditions. Below are the detailed steps for the preparation and the results of the comparative analysis.

Cryo-lift-out

Flat top silicon posts were prepared for lift-out by milling them at 0° stage tilt with a 30 kV 4 nA probe, corresponding to a 52° angle with respect to the specimen's normal, such that the apex diameter is approximately 5–6 μm and with an angled surface. This preliminary step was proposed by Schreiber et al. (2018) to maximize the surface contact between the lifted-out wedge and the post to strengthen the weld. If necessary, this step could be performed at room temperature prior to cooling the stage.

All further steps were done with the stage and micromanipulator at the lowest temperature setting (approximately 95 K). The undercut and lift-out procedure were carried out at 0° stage tilt in order to match the angle of the wedge with the prepared silicon post. A cantilever of 30 μm × 5 μm × 10 μm was prepared using milling patterns typically used for APT sample preparation, simply larger than typical (Thompson et al., 2007), Figure 1a, and with sufficiently large trenches to be able to observe the bottom of the cantilever during the undercut stage to ensure sample release. The manipulator was prepared through sharpening to a point less than 5 μm in diameter and placed in direct contact with a flat side parallel to the side of the cantilever to maximize the contact area for the subsequent redeposition. A series of 6–8 line or small and thin rectangle patterns were then milled across the interface between the manipulator and the cantilever such that a small amount of material is sputtered between them using a 30 kV 100 pA probe, forming a weld, which was referred to as a nanoweld by Schreiber et al. (2018). Only a small amount of material is required to make a connection that is mechanically sufficiently stable for the lift-out process and the exact probe current and size/shape of lines may vary with the relative sputtering rates of the two materials to be joined. This weld is expected to still be significantly less stable than a standard GIS glue section due to the lack of a continuous solid connection between the support structure and the sample material. Once welded, the arm of the cantilever is finally cut, and the wedge is lifted out, Figure 1a.

The wedge is then placed directly onto the prepared silicon post, Figure 1b, with care taken to align and make contact with the post in a single motion, as moving, making contact, and moving away from the post can cause the cantilever to pivot or break away due to, e.g., local Van der Waals forces or electrostatics from possible charging. Due to the fragile nature of this connection, any motion to the manipulator caused by the changing of FIB probe current aperture can be sufficient to cause sample loss, and so, it is recommended to not change the probe current if the specific changes cause vibration. Full thermalization of the stage carrying the sample holder, along with thermalization of the micromanipulator, should also be established before lift-out to avoid any degree of mechanical drift that could also stress the weld.

Experimentation showed that although the edges of wedges mounted in this way made sufficient connection to maintain stability, there can be significant gaps between the wedge and the post in the center. This reduces the contact area, which will reduce mechanical stability and electrical conductivity necessary for atom probe analysis. Here, once in place, and depending on the size of the wedge, a similar series of 4–8 lines (30 kV 0.1 nA for a line feature with a depth of 0.1 μm) were used to repeat the redeposition process on each of the four sides of the lifted-out wedge connecting to the post, Figure 1c. This redeposition stage is only to maintain stability of the interface for the next stage. Yet, care must be taken to only cause sufficient milling to connect the structures and not mill through the post. Indeed, the source of the redeposited material that connects the two structures originates from the milling away of the structures themselves. In order to ensure a stable connecting bridge, some but not all material from the adjacent edges of the structures must be milled away. The FIB probe conditions (30 kV, 100 pA, 0.1 μm × 1 μm × 0.1 μm) used here were able to provide sufficient levels of redeposition to connect to the two structures (tungsten and silicon) while not milling through either of the parts. These parameters would likely require optimization based upon the instrument used, focusing ability, available probe currents, and materials to be connected.

Once all four sides of the wedge have been connected to the post using redeposition, using the capability of the stage for full rotation, a trapezium-shaped region is milled from the side of the wedge such that the region-of-interest at the top of the wedge is retained. The manipulator is then inserted into this gap, Figure 2a, such that it is almost in contact with the wedge with a distance of a few hundred of nanometers. A cross-sectional, single-pass mill pattern at 30 kV 1 nA is then applied to the edge of the manipulator, with the ion beam rastering towards (pink arrow) the manipulator in order to maximize the sputtering from the manipulator and minimize the milling from the recently redeposited material. The precise conditions will depend on the currents available and the focusing ability of the probe current used on the instrument. The manipulator is then moved closer to maintain the distance between itself and the milled-out region and the milling process is repeated. The deposited material can be seen to slowly fill in the gap within the milled-out region and to have generally much contrast than the surrounding silicon, Figure 2b, with some contrast variations within it which imply some form of microstructure formed during deposition. For a manipulator with an end diameter of approximately 6 μm used herein, sufficient material was deposited within 10 min. For comparison, deposition of a 2 μm × 2 μm × 0.5 μm Pt using 12 kV 30 pA Xe^+ ions on either side of a lift-out standard wedge deposited on a commercial

Downloaded from https://academic.oup.com/mam/article/29/3/1009/7103332 by guest on 12 September 2023

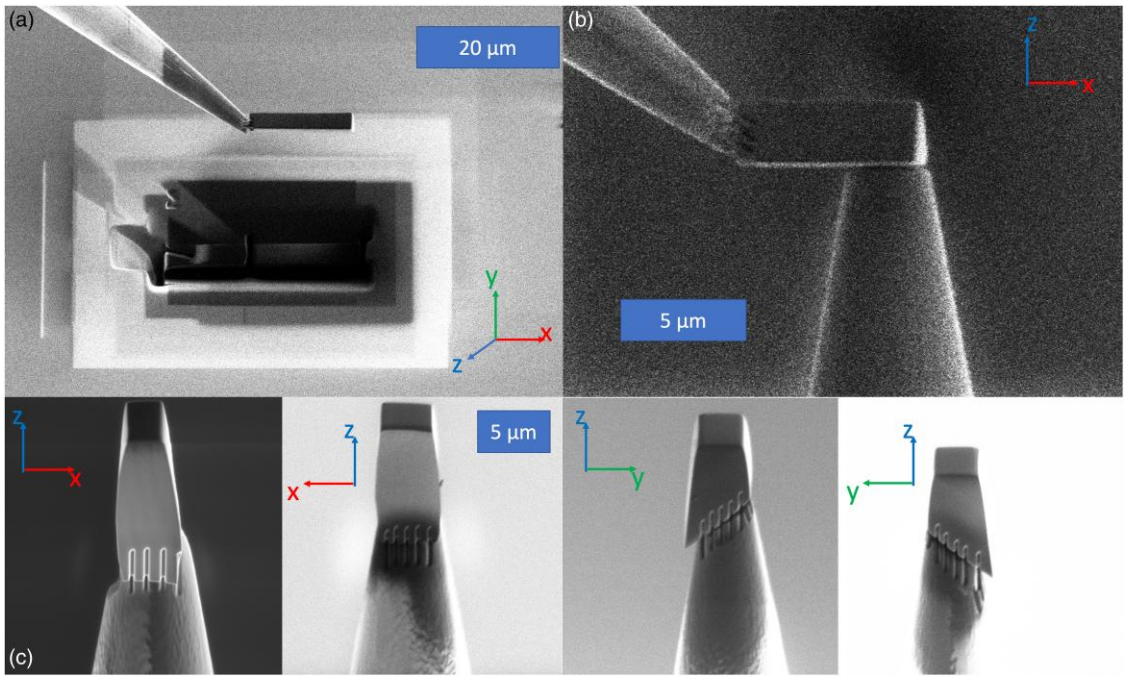


Fig. 1. (**a**) Cantilever containing the region-of-interest lifted out from the sample. The cantilever was attached by using redeposition. (**b**) Cantilever positioned onto the preshaped post of a commercial microtip coupon ready for attachment. (**c**) View of the weld by redeposition from the four sides performed in succession. Across all micrographs, the scale is given by the long axis of the rectangle.

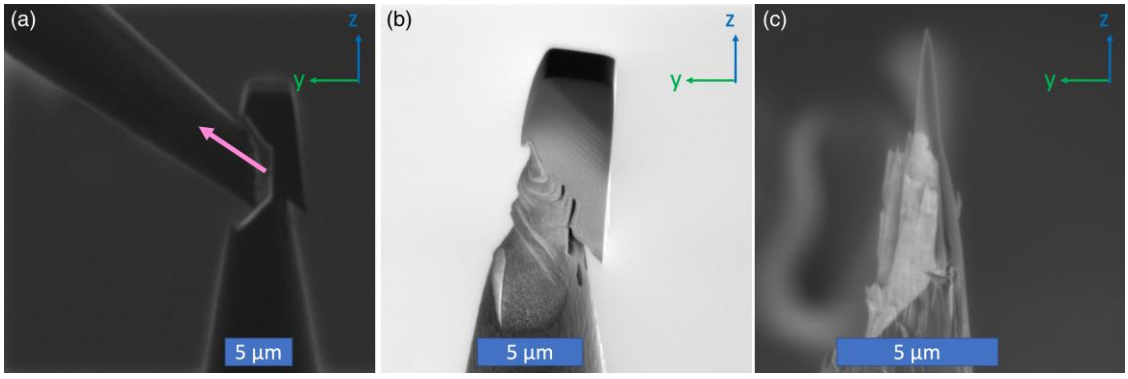


Fig. 2. (**a**) Insertion of the micromanipulator in the milled gap to enable the *in situ* strengthening weld. (**b**) Intermediate step with the W redeposited filling the gap. (**c**) Final specimen following needle shaping by annular milling; the W-weld is imaged brightly owing to the back-scattered contrast.

coupon requires approximately 6 min each side, and so the total time for this *in situ* deposition is similar.

Once sufficient redeposited material was in place to fill in the milled-out region, the sample was sharpened to an apex diameter less than 100 nm using 30 kV Xe^+ from 1 to 30 pA and polishing using 5 kV Xe^+ ions at 30 pA to remove regions severely damaged by the incoming energetic ion beam. Care was taken to ensure that minimal redeposited material was removed from the interface section to allow the largest possible volume of material for thermal and electrical conductivity. This was carried out by using annular milling with a relatively low current (30 kV, 0.3 nA, and below), reducing the inner diameter of the annulus quickly to reduce the amount of material removed from the bulk of the sample and carrying out the final sharpening using very short duration annular mills (1–2 s) to further reduce the amount of material removed from the bulk. The final specimen is shown in the micrograph in Figure 2c.

Transfer and Atom Probe Analysis

The sample was then allowed to warm up under vacuum within the chamber to room temperature before being transferred via the suitcase. Transfer at cryogenic temperature was avoided for this demonstration in order to remove the possibility of adsorbed gas species and other material onto these demonstration specimens during transport of a cooled sample through noncooled regions of the transfer route within the FIB and LEAP systems and facilitate the comparison with the presharpened microtip specimens. For a cryogenic transfer, the protocol would have been similar to what was reported previously in Stephenson et al. (2018), with a suitcase precooled by LN_2. Here, following transfer into the analysis chamber of the atom probe and data were collected.

The initial laser analysis using commonly used conditions showed comparable data quality in terms of peak shape to that collected by commercial silicon presharpened microtips, Figure 3a–b. This indicates that the overall thermal

Downloaded from https://academic.oup.com/mam/article/29/3/1009/7103332 by guest on 12 September 2023

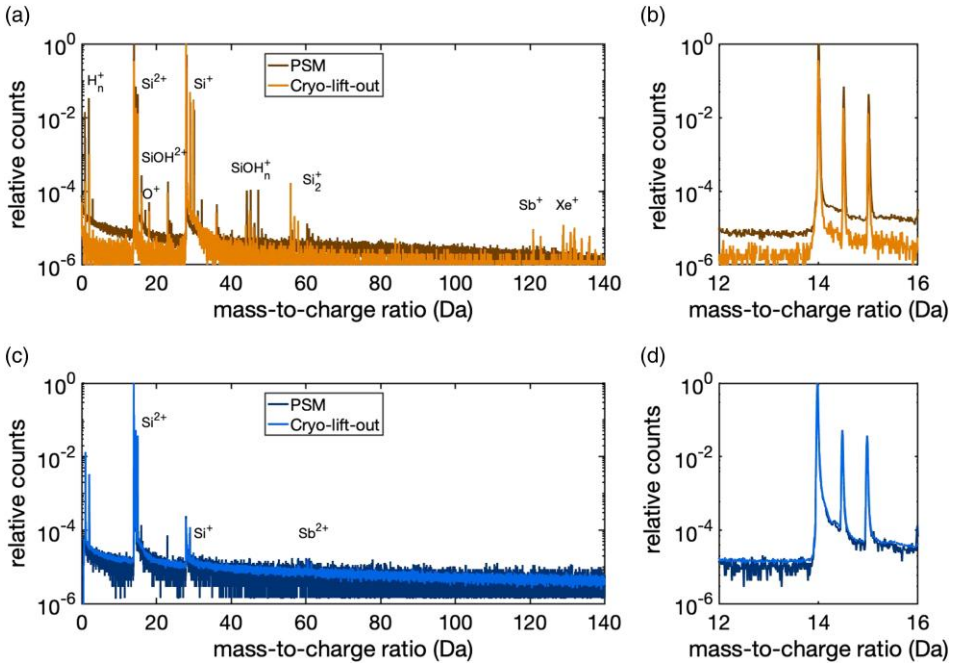


Fig. 3. Normalized mass spectra obtained from the analyses of a presharpened microtip (PSM) and specimens prepared by cryo-lift-out from the Sb-doped Si: (**a**) in laser-pulsing mode with (**b**) a close-up on the Si^{2+} peaks; (**c**) in high-voltage–pulsing mode with (**d**) a close-up on the Si^{2+} peaks.

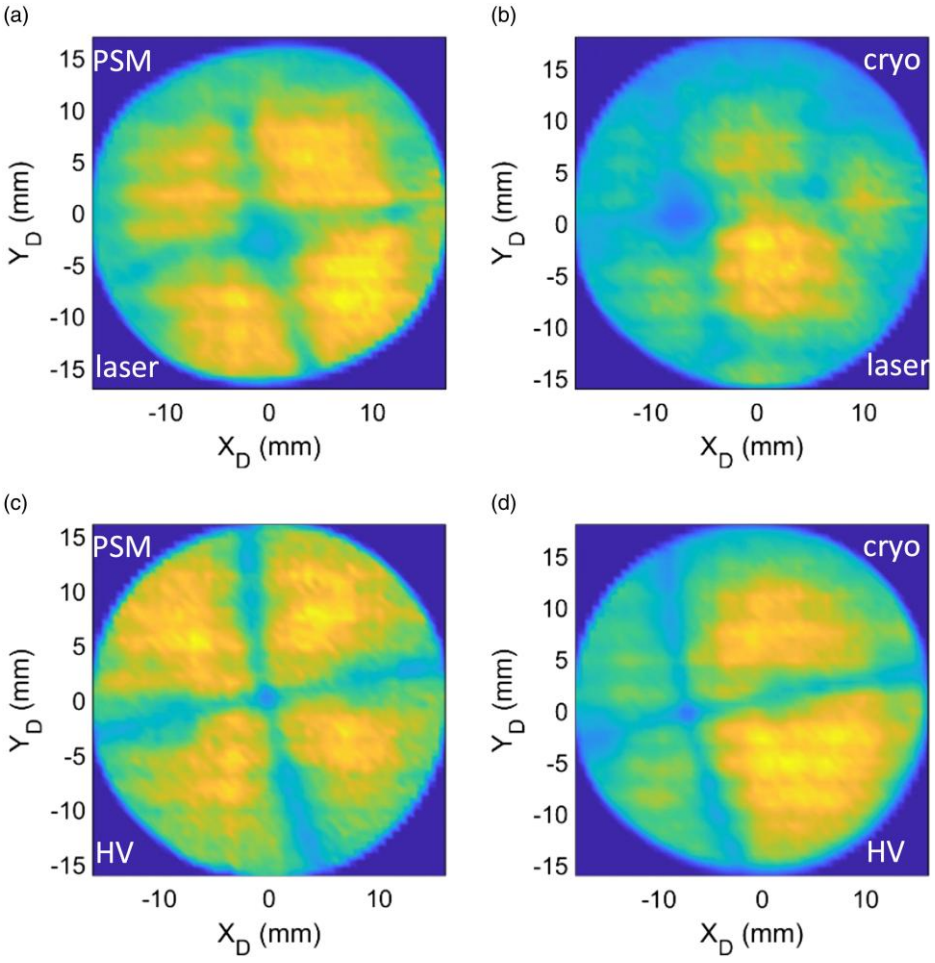


Fig. 4. Detector hit histogram from the analyses in laser-pulsing mode for (**a**) a presharpened microtip and (**b**) a specimen prepared by cryo-lift-out, and in voltage-pulsing mode for (**c**) a presharpened microtip and (**d**) a specimen prepared by cryo-lift-out.

Downloaded from https://academic.oup.com/mam/article/29/3/1009/7103332 by guest on 12 September 2023

conductivity of the sample, including the redeposited tungsten material, is sufficiently high to not cause visible "thermal tails" in the recorded data. The subsequent voltage-pulsing analysis, carried out up to a standing voltage of 9 kV with a pulse fraction of 20%, also showed comparable quality data to that collected from presharpened microtips, Figure 3c–3d. The sample survived analysis at voltages at the upper range of the requirements for most materials (approximately 11 kV), which can be taken as an indication that the mechanical stability of the sample is sufficient for the stresses associated with those voltages. The level of background in the mass spectrum obtained for the PSM is relatively higher, somehow closer to the level obtained with voltage pulsing. The higher proportion of Si^{2+} in the data set obtained from the PSM suggests that the background could be related to field evaporation triggered by the higher electrostatic field conditions (Kingham, 1982).

Finally, in Figure 4 are plotted the detector hit maps in laser (a–b) and HV mode (c–d) for both presharpened microtips and specimens prepared by cryo-lift-out. Since specimens were prepared from a [001]-oriented wafer, the fourfold symmetry of the (004) set of planes is readily visible in all maps. The position of the main pole in the map reveals the relative orientation of the lifted-out specimen with respect to the main specimen axis (*z* in Figs. 1 and 2) (Gault et al., 2012). We demonstrate here a reproducible and consistent positioning of lifted-out wedge with respect to the support. The difference in the apparent angular field-of-view and sharpness of the pole figure is simply related to the specimen's radius and analysis conditions (i.e., laser versus HV) as reported previously (Gault et al., 2010).

Discussion

Localized redeposition has been shown to be viable in the lift-out and mounting of TEM lamellae onto grids for cryo-TEM of frozen specimens (Kuba et al., 2020). This is where two features, typically a manipulator and lamella or a lamella and a grid arm, are placed in close proximity and an ion beam is used to remove small amounts of material from each side such that redeposits on and in-between the two features, forming a sufficiently stable bridge, i.e., a weld with sufficient mechanical stability to allow for further lamella thinning and TEM analysis. In routine for TEM—it is part of the routine training procedure by one of the leading brand of focused-ion beam microscopes—including at cryogenic temperatures, yet this process had not been optimized for APT specimen preparation. The requirements for APT specimens are rather different to TEM, and good electrical and thermal conductivities are required to ensure adequate analytical performance, along with sufficient strength to resist the extreme stresses during analysis (Wilkes et al., 1972; Kölling & Vandervorst, 2009; Moy et al., 2011).

The use of the tungsten micromanipulator as a localized sputtering source allows the use of a highly conductive and mechanical stable material for redeposition. It offers the major advantage that this can be performed at cryogenic temperature, and to lead to good adhesion, without the use of C-containing precursors or water, which can both be sources of contamination for some materials. In addition, the material that would normally be redeposited would be provided by the sample itself and in the case of frozen, hydrated samples, this could have significantly reduced electrical conductivity (Schreiber et al., 2018). *In situ* electrochemical charging and subsequent cryogenic sample transfer of atom probe samples prepared by lift-out have been shown to have issues with yield loss due to the room temperature GIS deposited weld and the replacement with redeposited pure metal could reduce sample failure (Khanchandani et al., 2022). Avoiding the requirement for a GIS for the lift-out protocol can be generalized for dual-beam instruments that have a micromanipulator but either no GIS or no functioning GIS.

The use of a precursor gas for local deposition is also a potential major source of carbon that can contaminate the surface, which can become critical in the correlative workflows where TEM and APT are combined on the same specimen (Herbig et al., 2015; Herbig, 2018; Spurgeon et al., 2018; Sasaki et al., 2022), that require careful cleaning as discussed extensively by Herbig & Kumar (2021). A GIS-free approach can hence be highly advantageous.

In the future, we expect to explore the use of this *in situ* deposition approach to perform coatings in presharpened specimens, which has been shown to be important for mechanical stability (Seol et al., 2016) and to enable environmental shielding from the environment along with electric field shielding that facilitate analysis of, e.g., Li-containing materials (Kim et al., 2022). At this stage, however, we do not know what the composition of the deposited material that forms the weld itself, and if it is amorphous or crystalline, if so, what its microstructure might be (e.g., grain size and orientation). It would be interesting to find out if Xe is being deposited as well, if it forms gaseous bubbles for instance, that might affect the mechanical stability of the weld, which would be difficult to assess by APT only. Finally, there remains many unknowns regarding how the deposition conditions can be adjusted to control the weld's composition and structure.

Tungsten is a standard material for micromanipulators due to its ease of manufacture using electrochemical polishing and resistance to ion milling, and it has a relatively low cost for replacement. However, manipulators could be manufactured from other metals that would be more suitable for redeposition or prefabricate (Kölling & Vandervorst, 2009). Multiple metals, such as aluminum and aluminum alloys, have been shown to be suitable for cryogenic sputter deposition (Chambers et al., 1988) and these will be trialed in the future.

Due to the increase in time required for sample preparation and the increase in width of the lift-out wedge to match the dimensions of the prepared support structure, it is unlikely that the full length of the lifted-out wedge would be usable. So it is likely that a reduction in the length of wedge can be carried out without reducing sample throughput. Preliminary steps such as the preparation of the micromanipulator or of the silicon post are not required to be carried out at cryogenic conditions, having a range of preprepared structures can be organized in advance, maybe even in a fully automated process. Prior to attachment, our approach only currently consists of a single, angled cut and there is scope for more elaborate prefabricated structures, such as an angled V cut or dovetail, that may be more suitable depending on the requirements for the sample and maybe its tendency for redepositing (Miller et al., 2005).

Conclusion

To conclude, we have demonstrated a methodology for the GIS-free, lift-out, and mounting of APT specimens at cryogenic temperatures, via selective redeposition of material from a

Downloaded from https://academic.oup.com/mam/article/29/3/1009/7103332 by guest on 12 September 2023

micromanipulator using commercially available instrumentation. This process has been showcased in the analysis of Sb-doped silicon specimens, with thermal and mechanical stability that compares with silicon reference material from pre-sharpened microtips. This approach can be readily adapted for use in a variety of cryogenic sample preparation of APT where existing GIS-based methods are not appropriate.

Availability of Data and Materials

The data is available on request from the authors.

Acknowledgments

Dr. Guillaume Amiard is acknowledged for fruitful discussions.

Financial Support

F.G. and B.G. are grateful for funding from the EPSRC under the grant # EP/V007661/1. B.G. is grateful for funding from the ERC for the project SHINE (ERC-CoG) #771602. M.C. acknowledges funding from the Royal Society Tata University Research Fellowship (URF\R1\201318) and the EPSRC NAME Programme Grant EP/V001914/1.

Conflict of Interest

The authors declare that they have no known competing financial interests or personal relationships that could have appeared to influence the work reported in this paper.

References

Anon (2017). https://www.nobelprize.org/prizes/chemistry/2017/press-release/ accessed 2020-05-26

Bhavsar SN, Aravindan S & Rao PV (2012). Experimental investigation of redeposition during focused ion beam milling of high speed steel. *Precis Eng* **36**, 408–413. https://doi.org/10.1016/j.precisioneng.2011.12.005

Blavette D, Cadel E & Deconihout B (2000). The role of the atom probe in the study of nickel-based superalloys. *Mater Charact* **44**, 133–157. https://doi.org/10.1016/S1044-5803(99)00050-9

Cairney JM & Munroe PR (2003). Redeposition effects in transmission electron microscope specimens of FeAl–WC composites prepared using a focused ion beam. *Micron* **34**, 97–107. https://doi.org/10.1016/S0968-4328(03)00007-6

Chambers DL, Wan CT, Susi GT & Taylor KA (1988). Sputtering deposition of thin films at cryogenic temperatures. *Surf Coat Technol* **36**, 893–900. https://doi.org/10.1016/0257-8972(88)90029-1

Chang Y, Lu W, Guénolé J, Stephenson LT, Szczpaniak A, Kontis P, Ackerman AK, Dear F, Mouton I, Zhong X, Raabe D, Gault B, Zhang S, Dye D, Liebscher CH, Ponge D, Korte-Kerze S, Raabe D & Gault B (2019). Ti and its alloys as examples of cryogenic focused ion beam milling of environmentally-sensitive materials. *Nat Commun* **10**, 942. https://doi.org/10.1038/s41467-019-08752-7

Clark DR, Zhu H, Diercks DR, Ricote S, Kee RJ, Almansoori A, Gorman BP & O'Hayre RP (2016). Probing grain-boundary chemistry and electronic structure in proton-conducting oxides by atom probe tomography. *Nano Lett* **16**, 6924–6930. https://doi.org/10.1021/acs.nanolett.6b02918

Conroy M, Soltis JA, Wittman RS, Smith FN, Chatterjee S, Zhang X, Ilton ES & Buck EC (2017). Importance of interlayer H bonding structure to the stability of layered minerals. *Sci Rep* **7**, 1–10. https://doi.org/10.1038/s41598-017-13452-7

Córdoba R, Orús P, Strohauer S, Torres TE & De Teresa JM (2019). Ultra-fast direct growth of metallic micro- and nano-structures by focused ion beam irradiation. *Sci Rep* **9**( ), 1–10. https://doi.org/10.1038/s41598-019-50411-w

de Geuser F & Gault B (2020). Metrology of small particles and solute clusters by atom probe tomography. *Acta Mater* **188**, 406–415. https://doi.org/10.1016/j.actamat.2020.02.023

Diercks DR, Gorman BP & Mulders JJL (2017). Electron beam-induced deposition for atom probe tomography specimen capping layers. *Microsc Microanal* **23**, 321–328. https://doi.org/10.1017/S1431927616011740

Dubochet J (2016). A reminiscence about early times of vitreous water in electron cryomicroscopy. *Biophys J* **110**, 756–757. https://doi.org/10.1016/j.bpj.2015.07.049

Dubochet J, Lepault J, Freeman R, Berriman JA & Homo J-C (1982). Electron microscopy of frozen water and aqueous solutions. *J Microsc* **128**, 219–237. https://doi.org/10.1111/j.1365-2818.1982.tb04625.x

El-Zoka AA, Kim SH, Deville S, Newman RC, Stephenson LT & Gault B. (2020). Enabling near-atomic-scale analysis of frozen water. *Sci Adv.* **6**(49), eabd6324. https://doi.org/10.1126/sciadv.abd6324

Famelton JR, Hughes GM, Williams CA, Barbatti C, Moody MP & Bagot PAJ (2021). Xenon plasma focussed ion beam preparation of an Al-6XXX alloy sample for atom probe tomography including analysis of an α-Al(Fe. Mn)Si dispersoid. *Mater Charact* **178**, 111194. https://doi.org/10.1016/j.matchar.2021.111194

Felfer PJ, Alam T, Ringer SP & Cairney JM (2012). A reproducible method for damage-free site-specific preparation of atom probe tips from interfaces. *Microsc Res Tech* **75**, 484–491. https://doi.org/10.1002/jemt.21081

Gault B, Chiaramonti A, Cojocaru-Mirédin O, Stender P, Dubosq R, Freysoldt C, Makineni SK, Li T, Moody M & Cairney JM (2021). Atom probe tomography. *Nat Rev Methods Primers* **1**(1), 51. https://doi.org/10.1038/s43586-021-00047-w

Gault B, La Fontaine A, Moody MPPMP, Ringer SPPSP & Marquis EAAEA (2010). Impact of laser pulsing on the reconstruction in an atom probe tomography. *Ultramicroscopy* **110**, 1215–1222. https://doi.org/10.1016/j.ultramic.2010.04.017

Gault B, Moody MP, Cairney JM & Ringer SP (2012). Atom probe crystallography. *Mater Today* **15**, 378–386. https://doi.org/10.1016/S1369-7021(12)70164-5

Grandfield K, Micheletti C, Deering J, Arcuri G, Tang T & Langelier B (2022). Atom probe tomography for biomaterials and biomineralization. *Acta Biomater* **148**, 44–60. https://doi.org/10.1016/j.actbio.2022.06.010

Haley D, London AJ & Moody MP (2020). Processing APT spectral backgrounds for improved quantification. *Microscopy and Microanalysis* **26**(5), 964–977. https://doi.org/10.1017/S1431927620024290

Halpin JE, Webster RWH, Gardner H, Moody MP, Bagot PAJ & MacLaren DA (2019). An in-situ approach for preparing atom probe tomography specimens by xenon plasma-focussed ion beam. *Ultramicroscopy* **202**, 121–127. https://doi.org/10.1016/j.ultramic.2019.04.005.

Henderson R, Baldwin JM, Ceska TA, Zemlin F, Beckmann E & Downing KH (1990). Model for the structure of bacteriorhodopsin based on high-resolution electron cryo-microscopy. *J Mol Biol* **213**, 899–929. https://doi.org/10.1016/S0022-2836(05)80271-2

Herbig M (2018). Spatially correlated electron microscopy and atom probe tomography: Current possibilities and future perspectives. *Scr Mater* **148**, 98–105. https://doi.org/10.1016/j.scriptamat.2017.03.017

Herbig M, Choi P & Raabe D (2015). Combining structural and chemical information at the nanometer scale by correlative transmission electron microscopy and atom probe tomography. *Ultramicroscopy* **153**, 32–39. https://doi.org/10.1016/j.ultramic.2015.02.003

Herbig M & Kumar A (2021). Removal of hydrocarbon contamination and oxide films from atom probe specimens. *Microsc Res Tech* **84**, 291–297. https://doi.org/10.1002/jemt.23587

Downloaded from https://academic.oup.com/mam/article/29/3/1009/7103332 by guest on 12 September 2023

Jenkins BM, Danoix F, Gouné M, Bagot PAJ, Peng Z, Moody MP & Gault B (2020). Reflections on the analysis of interfaces and grain boundaries by atom probe tomography. *Microsc Microanal* **26**, 247–257. https://doi.org/10.1017/S1431927620000197

Kelly TF, Larson DJ, Thompson K, Alvis RL, Bunton JH, Olson JD & Gorman BP (2007). Atom probe tomography of electronic materials. *Annu Rev Mater Res* **37**, 681–727. https://doi.org/10.1146/annurev.matsci.37.052506.084239

Khanchandani H, Kim S-H, Varanasi RS, Prithiv T, Stephenson LT & Gault B (2022). Hydrogen and deuterium charging of lifted-out specimens for atom probe tomography. *Open Res Europe* **1**, 122. https://doi.org/10.12688/openreseurope.14176.2

Kim S, Antonov S, Zhou X, Stephenson L, Jung C, El-Zoka A, Schreiber DK, Conroy S, Gault B, Mater J, Kim S-H, Antonov S, Zhou X, Stephenson LT, Jung C, El-Zoka AA, Schreiber DK, Conroy M & Gault B (2022). Atom probe analysis of electrode materials for Li-ion batteries: Challenges and ways forward. *J Mater Chem A* **6**, 4883–5230.

Kingham DR (1982). The post-ionization of field evaporated ions: A theoretical explanation of multiple charge states. *Surf Sci* **116**, 273–301. https://doi.org/10.1016/0039-6028(82)90434-4

Kölling S & Vandervorst W (2009). Failure mechanisms of silicon-based atom-probe tips. *Ultramicroscopy* **109**, 486–491. https://doi.org/10.1016/j.ultramic.2008.11.013

Kuba J, Mitchels J, Hovorka M, Erdmann P, Berka L, Kirmse R, König J, De Bock J, Goetze B & Rigort A (2021). Advanced cryo-tomography workflow developments—Correlative microscopy, milling automation and cryo-lift-out. *J Microsc.* **281**(2), 112–124. https://doi.org/10.1111/jmi.12939

Kumar S, Wang Z, Lee Perm R & Tsapatsis M (2008). A structural resolution cryo-TEM study of the early stages of MFI growth. *J Am Chem Soc* **130**, 17284–17286. https://doi.org/10.1021/ja8063167

Larson DJ, Foord DT, Petford-Long AK, Anthony TC, Rozdilsky IM, Cerezo A & Smith GWD (1998). Focused ion-beam milling for field-ion specimen preparation. *Ultramicroscopy* **75**, 147–159. https://doi.org/10.1016/S0304-3991(98)00058-8

Lilensten L & Gault B (2020). New approach for FIB-preparation of atom probe specimens for aluminum alloys. *PLoS One* **15**(4), e0231179. https://doi.org/10.1371/journal.pone.0231179

Marquis EA, Bachhav M, Chen Y, Dong Y, Gordon LM & McFarland A (2013). On the current role of atom probe tomography in materials characterization and materials science. *Curr Opin Solid State Mater Sci* **17**, 217–223. https://doi.org/10.1016/j.cossms.2013.09.003

Matteson TL, Schwarz SW, Houge EC, Kempshall BW & Giannuzzi LA (2002). Electron backscattering diffraction investigation of focused ion beam surfaces. *J Electron Mater* **31**, 33–39. https://doi.org/10.1007/s11664-002-0169-5

Mayer J, Giannuzzi LA, Kamino T & Michael J (2007). TEM sample preparation and damage. *MRS Bull* **32**, 400–407. https://doi.org/10.1557/mrs2007.63

Miller MK, Russell KF & Thompson GB (2005). Strategies for fabricating atom probe specimens with a dual beam FIB. *Ultramicroscopy* **102**, 287–298. https://doi.org/10.1016/j.ultramic.2004.10.011

Montoya E, Bals S, Rossell MD, Schryvers D & Van Tendeloo G (2007). Evaluation of top, angle, and side cleaned FIB samples for TEM analysis. *Microsc Res Tech* **70**, 1060–1071. https://doi.org/10.1002/jemt.20514

Mouton I, Chang Y, Chakraborty P, Wang S, Stephenson LT, ben Britton T & Gault B (2021). Hydride growth mechanism in zircaloy-4: Investigation of the partitioning of alloying elements. *Materialia* **15**, 101006. https://doi.org/10.1016/j.mtla.2021.101006

Moy CKS, Ranzi G, Petersen TC & Ringer SP (2011). Macroscopic electrical field distribution and field-induced surface stresses of needle-shaped field emitters. *Ultramicroscopy* **111**, 397–404. https://doi.org/10.1016/j.ultramic.2011.01.024

Nobel Prize ®and the Nobel Prize ®medal design mark are registrated trademarks of the Nobel Foundation Scientific Background on the Nobel Prize in Chemistry 2017 THE DEVELOPMENT OF CRYO-ELECTRON MICROSCOPY (2017). https://www.nobelprize.org/prizes/chemistry/2017/summary/.

Orús P, Sigloch F, Sangiao S & De Teresa JM (2021). Cryo-focused ion beam-induced deposition of tungsten–carbon nanostructures using a thermoelectric plate. *Appl Sci* **11**, 10123. https://doi.org/10.3390/app112110123

Park YK, Nagai T, Takai M, Lehrer C, Frey L & Ryssel H (1999). Microanalysis of FIB induced deposited Pt films using ion microprobe. *Proc Int Conf Ion Implant Technol* **2**, 1137–1139.

Parmenter CD & Nizamudeen ZA (2021). Cryo-FIB-lift-out: Practically impossible to practical reality. *J Microsc* **281**(2), 157–174. https://doi.org/10.1111/jmi.12953

Perea DE, Gerstl SSA, Chin J, Hirschi B & Evans JE (2017). An environmental transfer hub for multimodal atom probe tomography. *Adv Struct Chem Imaging* **3**, 12. https://doi.org/10.1186/s40679-017-0045-2

Prosa TJ & Larson DJ (2017). Modern focused-ion-beam-based site-specific specimen preparation for atom probe tomography. *Microsc Microanal* **23**, 194–209. https://doi.org/10.1017/S1431927616012642

Rajsiri S, Kempshall BW, Schwarz SM & Giannuzzi LA (2002). FIB damage in silicon: Amorphization or redeposition? *Microsc Microanal* **8**, 50–51. https://doi.org/10.1017/S1431927602101577

Revealed I, Yuwono VM, Burrows ND, Soltis JA & Lee Penn R (2010). Oriented aggregation: Formation and transformation of mesocrystal. *J Am Chem Soc* **132**, 2163–2165. https://doi.org/10.1021/ja909769a

Ringer S (2006). Recent advances in atom probe tomography and applications to understanding nanomaterials. *Microsc Microanal* **12**, 220–221. https://doi.org/10.1017/S1431927606068206

Salvador-Porroche A, Sangiao S, Philipp P, Cea P & de Teresa JM (2020). Optimization of Pt-C deposits by cryo-FIBID: Substantial growth rate increase and quasi-metallic behaviour. *Nanomaterials* **10**, 1906. https://doi.org/10.3390/nano10101906

Sasaki TT, Sepehri-Amin H, Uzuhashi J, Ohkubo T & Hono K (2022). Complementary and correlative (S)TEM/APT analysis of functional and structural alloys. *MRS Bull* **47**, 688–695. https://doi.org/10.1557/s43577-022-00374-7

Saxey DW, Moser DE, Piazolo S, Reddy SM & Valley JW (2018). Atomic worlds: Current state and future of atom probe tomography in geoscience. *Scr Mater* **148**, 115–121. https://doi.org/10.1016/j.scriptamat.2017.11.014

Schreiber DK, Perea DE, Ryan JV, Evans JE & Vienna JD (2018). A method for site-specific and cryogenic specimen fabrication of liquid/solid interfaces for atom probe tomography. *Ultramicroscopy* **194**, 89–99. https://doi.org/10.1016/j.ultramic.2018.07.010

Seol JB, Kwak CM, Kim YT & Park CG (2016). Understanding of the field evaporation of surface modified oxide materials through transmission electron microscopy and atom probe tomography. *Appl Surf Sci* **368**, 368–377. https://doi.org/10.1016/j.apsusc.2016.01.196

Spurgeon SR, Sushko PV, Devaraj A, Du Y, Droubay T & Chambers SA (2018). Onset of phase separation in the double perovskite oxide La_2MnNiO_6. *Phys Rev B* **97**, 134110. https://doi.org/10.1103/PhysRevB.97.134110

Stephenson LT, Szczepaniak A, Mouton I, Rusitzka KAK, Breen AJ, Tezins U, Sturm A, Vogel D, Chang Y, Kontis P, Rosenthal A, Shepard JD, Maier U, Kelly TF, Raabe D & Gault B (2018). The Laplace project: An integrated suite for correlative atom probe tomography and electron microscopy under cryogenic and UHV conditions. *PLoS One* **13**, e0209211.

Taylor KA & Glaeser RM (1974). Electron diffraction of frozen, hydrated protein crystals. *Science* **186**, 1036–1037. https://doi.org/10.1126/science.186.4168.1036

Taylor KA & Glaeser RM (1976). Electron microscopy of frozen hydrated biological specimens. *J Ultrastruct Res* **55**, 448–456. https://doi.org/10.1016/S0022-5320(76)80099-8

Thompson K, Lawrence D, Larson DJ, Olson JD, Kelly TF & Gorman B (2007). In situ site-specific specimen preparation for atom probe tomography. *Ultramicroscopy* **107**, 131–139. https://doi.org/10.1016/j.ultramic.2006.06.008

Downloaded from https://academic.oup.com/mam/article/29/3/1009/7103332 by guest on 12 September 2023

van Dorp WF, Wnuk JD, Gorham JM, Fairbrother DH, Madey TE & Hagen CW (2009). Electron induced dissociation of trimethyl (methylcyclopentadienyl) platinum (IV): Total cross section as a function of incident electron energy. *J Appl Phys* **106**, 074903. https://doi.org/10.1063/1.3225091

Wilkes TJ, Titchmar JM, Smith GDW, Smith DA, Morris RF, Johnston S, Godfrey TJ & Birdseye P (1972). Fracture of field-ion microscope specimens. *J Phys D Appl Phys* **5**, 2226–2230. https://doi.org/10.1088/0022-3727/5/12/312

Winter DAMd & Mulders JJL (2007). Redeposition characteristics of focused ion beam milling for nanofabrication. *J Vac Sci Technol B Microelectron Nanometer Struct Process Measure Phenom* **25**, 2215.

Zachman MJ, Tu Z, Choudhury S, Archer LA & Kourkoutis LF (2018). Cryo-STEM mapping of solid–liquid interfaces and dendrites in lithium-metal batteries. *Nature* **560**, 345–349. https://doi.org/10.1038/s41586-018-0397-3.

Zhong XL, Haigh SJ, Zhou X & Withers PJ (2020). An in-situ method for protecting internal cracks/pores from ion beam damage and reducing curtaining for TEM sample preparation using FIB. *Ultramicroscopy* **219**, 113135. https://doi.org/10.1016/j.ultramic.2020.113135

Zhu G, Sushko ML, Loring JS, Legg BA, Song M, Soltis JA, Huang X, Rosso KM & de Yoreo JJ (2021). Self-similar mesocrystals form via interface-driven nucleation and assembly. *Nature* **590**, 416–422. https://doi.org/10.1038/s41586-021-03300-0

Downloaded from https://academic.oup.com/mam/article/29/3/1009/7103332 by guest on 12 September 2023